The Electronic Structures of Active Sites in Non-Heme Iron Enzymes

EDWARD I. SOLOMON* and YAN ZHANG

Department of Chemistry, Stanford University, Stanford, California 94305

Received January 17, 1992

A large number of mononuclear and binuclear non-heme iron enzymes perform a variety of important biological functions often involving the binding and activation of dioxygen by the reduced (i.e., ferrous) form of the metalloprotein active site. These include the oxygen-binding protein hemerythrin, dioxygenases, monooxygenases, oxidases, and the DNA-cleaving anticancer drug bleomycin. A major goal of our research has been to use spectroscopy to probe the geometric and electronic structure of the iron active site and its interactions with substrate and dioxygen. This has provided molecular level insight into the catalytic mechanisms and defined structural differences among enzymes which relate to differences in function. Spectral studies on non-heme Fe(II) active sites have been particularly challenging as these are high-spin $S = 2$ non-Kramers ions and thus in many cases do not exhibit EPR signals, and also do not have intense ligand-to-metal charge-transfer transitions in the visible region of the absorption spectrum. However, the Fe(II) ion has an open-shell d^6 electronic configuration which generates a number of low-lying, weak, ligand field excited states. We have applied a combination of electronic absorption (Abs), circular dichroism (CD) and magnetic circular dichroism (MCD) spectroscopies to observe these ligand field transitions in Fe(II) enzymes and model complexes, and we have further used the temperature and field dependence of the MCD spectrum to probe the ground-state sublevel splittings even for Fe(II) centers which do not exhibit EPR signals. The latter is analyzed in terms of a non-Kramers spin-Hamiltonian formalism, and the parameters obtained are further interpreted in terms of ligand field theory. Together these studies provide the experimental splitting of the d orbitals of the metal center, which probes its geometric and electronic structure, and in the binuclear systems, determine the exchange coupling between the metal centers, which provides significant insight into bridging ligation. In the first part of this Account, we develop this excited-state spectroscopic approach focusing on the mononuclear Fe(II) centers in superoxide dismutase and lipoxygenase (an enzyme catalyzing the hydroperoxidation of fatty acids).

Excited-State Spectroscopic Protocol: Fe(II) Superoxide Dismutase and Lipoxygenase

The Fe(II) free ion has a ^5D state lowest in energy which splits in an octahedral ligand field into a 3-fold orbitally degenerate $^5T_{2g}$ ground state and a 2-fold degenerate ^5E_g excited state. This octahedral state splitting corresponds to a one-electron-orbital change as the $^5T_{2g}$ state has a $(t_{2g})^4(e_g)^2$ configuration and the ^5E_g a $(t_{2g})^3(e_g)^3$ configuration. The energy level diagram in Figure 1 results in one spin-allowed $^5T_{2g} \rightarrow {}^5E_g$ ligand field transition at $10Dq_{O_h}$, which is in the range of 10 000–11 000 cm^{-1} for biologically relevant nitrogen and oxygen ligation in a six-coordinate environment.[1] The ^5E_g excited state will split in lower symmetries by an amount Δ^5E_g, which corresponds to the energy difference between the d_{z^2} and $d_{x^2-y^2}$ orbitals. In a distorted six-coordinate site, this splitting will be <2000 cm^{-1}, while in a five-coordinate square pyramidal structure it will be >5000 cm^{-1}, resulting in one ligand field transition at >10 000 cm^{-1} and a second at ~5000 cm^{-1} in the near-infrared (IR) spectral region.[2] For a five-coordinate trigonal bipyramidal structure the splitting pattern changes,[3] with the highest energy ligand field transition now at <10 000 cm^{-1} and the lower energy band at <5000 cm^{-1}. In a tetrahedral structure the ligand field splitting of the d orbitals is $10Dq_{T_d} = -{}^4/_9(10Dq_{O_h})$, and the spin-allowed $^5E \rightarrow {}^5T_2$ transition[4] will be at ~5000 cm^{-1}. From this correlation it is clear that the energies of the ligand field excited states are sensitive probes of the coordination environment of the Fe(II) site. Note that in Figure 1 the $^5T_{2g}$ ground state splitting, which is defined by the parameters Δ and v, also changes with geometric structure (vide infra). However, this will be much smaller than the Δ^5E_g splitting since the ground-state splitting reflects differences in π rather than σ interactions with the ligands.

Abs, CD, and low-temperature MCD data[5] in the ligand field region for Fe(II) superoxide dismutase (SOD) and soybean lipoxygenase (SBL) are presented in Figure 2. Each excited-state spectral method is governed by different selection rules (the dichroism

Edward I. Solomon is the Monroe E. Spaght Professor of Chemistry at Stanford University, where he has been since 1982, and was previously a professor at the Massachusetts Institute of Technology. He received his Ph.D. for research directed by Professor Donald S. McClure at Princeton University, and then he was a postdoctoral fellow working first with Professor C. J. Ballhausen at the H. C. Ørsted Institute at the University of Copenhagen and then with Professor Harry B. Gray at the California Institute of Technology. He is an associate editor of *Inorganic Chemistry* and a member of the editorial advisory boards of *Chemical Reviews* and *Inorganic Biochemistry*. He was the first Glen Seaborg, O. K. Rice, Reilly, Frontiers and World Bank lecturer, and he received the 1990 Deans Award for Distinguished Teaching. His research interests include physical–inorganic chemistry, bioinorganic chemistry, and surface science with emphasis on the detailed spectroscopic study of transition metal ion electronic structure.

Yan Zhang is currently completing her Ph.D. degree with Prof. Solomon at Stanford University. She received her B.S. from Peking University in 1982 and then worked as a chemical engineer on the development of industrial catalysts at Beijing Research Institute of Chemical Industry. Her current research is on the applications of a variety of spectroscopic methods to problems in non-heme iron chemistry.

(1) Lever, A. B. P. *Inorganic Electronic Spectroscopy*; Elsevier: New York, 1984; pp 458–467.

(2) (a) Nicholls, D. *The Chemistry of Iron, Cobalt and Nickel*; Pergamon: New York, 1973; pp 979–1051. (b) Goedken, V. L.; Merrell, P. H.; Busch, D. H. *J. Am. Chem. Soc.* **1972**, *94*, 3397.

(3) Ciampolini, M.; Nardi, N. *Inorg. Chem.* **1966**, *5*, 1150–1154.

(4) Forster, D.; Goodgame, D. M. L. *J. Chem. Soc.* **1965**, 454–458.

(5) (a) Whittaker, J. W.; Solomon, E. I. *J. Am. Chem. Soc.* **1986**, *108*, 835–836. (b) Whittaker, J. W.; Solomon, E. I. *J. Am. Chem. Soc.* **1988**, *110*, 5329–5339.

0001-4842/92/0125-0343$03.00/0

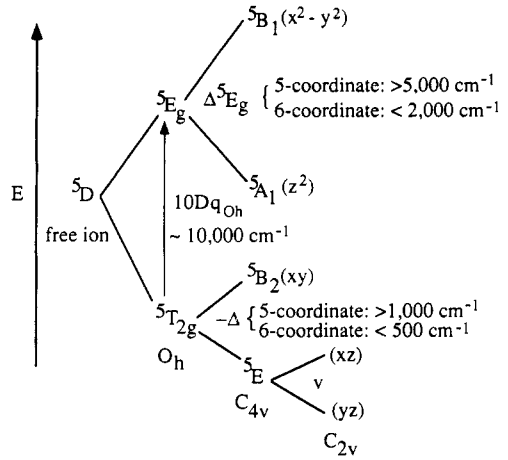

Figure 1. Energy level diagram of the ligand field splitting of the Fe(II) quintet states. These states correspond to having the extra electron of the d^6 configuration occupy the d orbital indicated in parentheses.

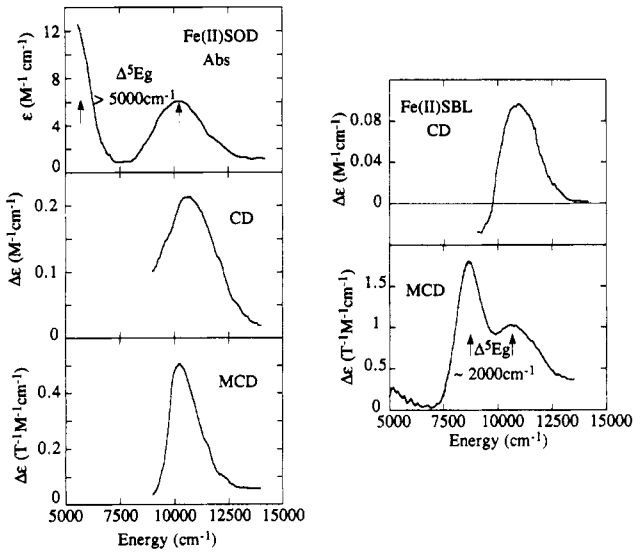

Figure 2. Ligand field spectra for the Fe(II) sites in superoxide dismutase (left) and soybean lipoxygenase (right). Arrows indicate the approximate positions of each ligand field transition. Note that the MCD spectral range for SBL has been extended from that in ref 5 with new instrumentation.

methods having a sign as well as an intensity), thus allowing the maximum resolution of the spectrum. Fe(II) SOD exhibits one transition at >10 000 cm^{-1} and a second at <6000 cm^{-1} clearly indicating an approximately square pyramidal structure for this active site. The crystal structure of the ferric SOD active site also indicates a five-coordinate structure for the oxidized site, but its geometry is described as being closer to trigonal bipyramidal.[6] For SBL, the Abs is too weak to be observed ($\epsilon < 1$ M^{-1} cm^{-1}). However, the CD and low-temperature MCD spectra clearly show two ligand field transitions in the ~10 000-cm^{-1} region split by ~2000 cm^{-1}, indicating a distorted octahedral geometry at the Fe(II) SBL active site.

We have further used variable temperature, variable field MCD to probe the ground states of these Fe(II) active sites.[5] The basis for this experiment is summarized in Figure 3 for the simplest case of a total angular

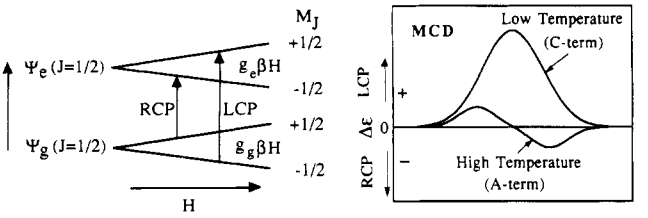

Figure 3. Magnetic circular dichroism selection rules. Left: transitions between Zeeman-split J (or S) = $^1/_2$ paramagnetic ground (g) and excited (e) states (RCP = right circularly polarized light; LCP = left circularly polarized light). Right: MCD spectra associated with the energy scheme on the left. Parallel to an absorption band, the C-term spectrum corresponds to a Gaussian bandshape, while an A-term reflects its first derivative.

momentum J (or S) = $^1/_2$ ion. Just as in an EPR experiment, both the ground (Ψ_g) and excited (Ψ_e) states will split in a magnetic field by an amount $g\beta H$. From the selection rules for the MCD experiment ($\Delta M = +1$ for left and -1 for right circular polarization), one predicts two transitions of equal intensity but opposite sign to a given excited state. Since transitions to excited states are generally a few thousand inverse centimeters wide due to vibronic coupling while $g\beta H$ is on the order of 10 cm^{-1} for the 6–7-T magnetic fields used in the MCD experiment, the two MCD transitions will mostly cancel, producing a broad, weak, derivative-shaped dichroism signal called an A-term[7] (Figure 3, right). This A-term spectrum is observed only in the high-temperature limit where both M_J (or M_s) components of the ground state are equally populated. When the temperature is lowered, the population of the $+^1/_2$ component is depleted, and cancellation no longer occurs. In the example illustrated in Figure 3, left, this would result in a left circularly polarized (LCP) MCD signal known as a C-term[7] which increases in intensity with decreasing temperature ($I_{MCD} \propto 1/T$) as long as $kT > g\beta H$. It should be noted that this C-term temperature dependent MCD intensity mechanism requires a degenerate ground state which is split in energy by application of a magnetic field.

A particularly interesting behavior occurs at very low temperature and high magnetic field where only the $-^1/_2$ component of the ground state has significant Boltzmann population. In this case the MCD signal no longer increases with decreasing temperature or increasing magnetic field and is said to be saturated.[8] The variable field MCD data for a fixed low temperature for the 10 400-cm^{-1} ligand field band of Fe(II) SOD (Figure 2) are given in Figure 4A. Note that the incremental increase in the MCD signal decreases with increasing magnetic field, eventually leveling off above 5 T, which reflects this saturation behavior. Saturation magnetization curves for Fe(II) SOD[5] taken at several different temperatures are given in Figure 4B, which presents the MCD amplitude of the 10 400-cm^{-1} band as a function of $\beta H/2kT$. If the ground state were an isolated S = $^1/_2$ doublet as in Figure 3, these curves would superimpose rather than exhibiting the nested behavior[9] in Figure 4B. High-spin Fe(II) has an S = 2 ground state which can undergo a zero (magnetic)

(6) Stallings, W. C.; Pattridge, K. A.; Ludwig, M. L. In *Superoxide and Superoxide Dismutase in Chemistry, Biology, and Medicine*; Rotilio, G., Ed.; Elsevier: New York, 1986.

(7) (a) Buckingham, A. D.; Stephens, P. J. *Annu. Rev. Phys. Chem.* **1966**, *171*, 399. (b) Piepho, S. B.; Schatz, P. N. *Group Theory in Spectroscopy*; Wiley: New York, 1983.

(8) Schatz, P. N.; Mowery, R. L.; Krausz, E. R. *Mol. Phys.* **1978**, *35*, 1537–1557.

(9) Thompson, A. J.; Johnson, M. K. *Biochem. J.* **1980**, *191*, 411–420.

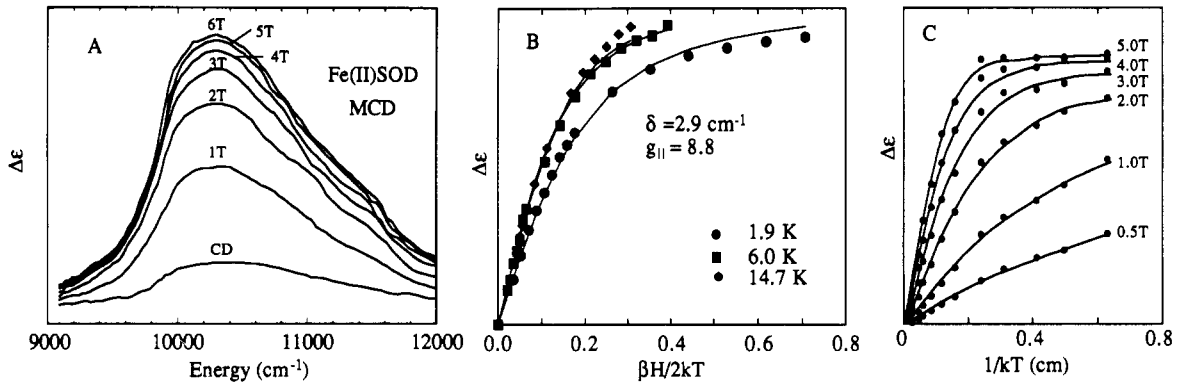

Figure 4. Temperature and magnetic field dependent MCD as a probe to the ground state of Fe(II) SOD. (A) Magnetic field dependent MCD data at 4.2 K showing saturation behavior. (B) Saturation magnetization curves: the MCD transition amplitude (as in A) for a range of magnetic fields (0–6 T) at a series of fixed temperatures is plotted as function of $\beta H/2kT$. (C) A replot of saturation data in B as function of temperature at a series of fixed magnetic fields. Note that the MCD amplitude at lowest temperature (i.e., to the right) increases with increasing magnetic field in a nonlinear fashion.

Table I
Experimental Ground-State Splittings and Ligand Field Parameters

		model complexes		
	Fe(II) SOD	C_{4v}	O_h	Fe(II) SBL
δ (cm^{-1})	2.9	1.3	8.3	7.2
$g_\parallel$	8.8	9.0	8.6	8.2
$-\Delta$ (cm^{-1})	1200 ± 300	2000 ● 500	250 ± 100	450 ± 100
$v/2\Delta$	0.27 ± 0.05	0.15 ± 0.02	0.30 ± 0.05	0.30 ± 0.05

field splitting (ZFS) due to the axial (D) and rhombic (E) components of the ligand field as described by the spin Hamiltonian in eq 1. As shown to the left in

$$\mathcal{H} = D[(S_z)^2 - (1/3)S(S+1)] + E[(S_x)^2 + (S_y)^2] \quad (1)$$

Figure 5, the axial term splits the $S = 2$ state into $M_s = 0, \pm1$ (at D), and ±2 (at $4D$) sublevels, the order depending on the sign of D. It had been thought that the nesting of MCD saturation magnetization curves for $S > {}^1/_2$ systems derives from the Boltzmann population of higher sublevels of the ground state.[9] At this point it should be emphasized that the Fe(II) center is a non-Kramers ion with an integer spin. Thus the $M_s = \pm2$ and $M_s = \pm1$ components can also be zero field split due to the rhombic component of the ligand field. It is this rhombic splitting of the $\pm M_s$ sublevels (Figure 5) which often leads to the lack of an EPR signal in non-Kramers ions.

Further insight into the origin of the nested behavior in Figure 4B was derived from the new plot in Figure 4C, which gives the MCD amplitude at a series of fixed magnetic fields with decreasing temperature.[5] For a given magnetic field the MCD intensity increases with decreasing temperature, suggesting that it arises from a C-term mechanism which would require a paramagnetic doublet ground state; that is, the $M_s = \pm2$ component of the ground state would be lowest in energy, corresponding to a negative D in Figure 5. However, Figure 4C shows that the MCD amplitude at low temperature (where only the lowest component of this doublet is populated) increases with increasing magnetic field, approaching a limiting value at high fields. This behavior, in fact, corresponds to a temperature dependent nonlinear B-term and requires that the wavefunction of the lowest sublevel changes with increasing magnetic field. We have explained this effect in terms of the model in Figure 5, right, where a rhombic splitting of the $M_s = \pm2$ ground state at zero magnetic field, δ, results in real wavefunctions $|X\rangle$ and $|Y\rangle$ which have equal mixtures of the MCD active $|+2\rangle$ and $|-2\rangle$ functions ($|X\rangle = (1/2^{1/2})[|+2\rangle + |-2\rangle]$, $|Y\rangle = (1/2^{1/2})[|+2\rangle - |-2\rangle]$) which are of opposite MCD sign and cancel. As the magnetic field increases, these wavefunctions change (and the levels split further in energy by $g_\parallel \beta H \cos\theta$, where θ is the angle between the magnetic field and the molecular z axis) to become purely complex and thus MCD active at magnetic fields greater than the rhombic splitting. The important point to emphasize in this analysis is that *it is the magnetic field induced mixing of the wavefunctions within a rhombically split non-Kramers doublet which is the origin of the nesting behavior of the saturation magnetization curves in Figure 4B.* Quantitatively, this behavior is described by eq 6 in ref 5b, which gives the MCD intensity as a function of magnetic field and temperature averaged over all molecular orientations in a frozen glass sample. Fitting the Fe(II) SOD data to this expression gives the solid lines in Figure 4B,C and values for δ and $g_\parallel$ which are given in Table I. Analogous data have been obtained and analyzed for Fe(II) SBL and for six-coordinate (O_h) and five-coordinate (C_{4v}) Fe(II) model complexes, and the parameters obtained are included in Table I. From Table I, Fe(II) SOD and the five-coordinate complex have small values of δ (and a relatively large $g_\parallel$) while Fe(II) SBL and the six-coordinate com-

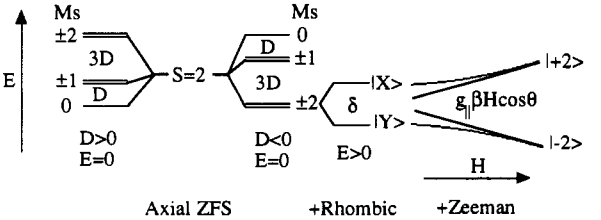

Figure 5. Energy level diagram for a $S = 2$ state. Left to right: effects of positive and negative axial zero field splitting, rhombic splitting of the non-Kramers ±2 doublet, Zeeman effect on this doublet.

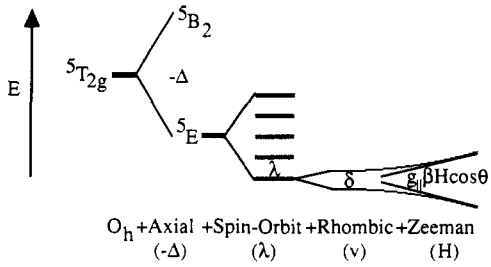

Figure 6. Energy level diagram for the $^5T_{2g}$ octahedral ground state. *Left to right: effect of the axial component of the ligand field on the orbital triplet, in-state spin–orbit coupling between the $S = 2$ and the axial orbital E, effect of the rhombic component of the ligand field on the lowest non-Kramers doublet, Zeeman splitting of this doublet.*

plex have large values of δ.

The information content of these $S = 2$ spin-Hamiltonian parameters (δ and $g_\parallel$) in terms of the splittings of the d_{xy}, d_{xz}, d_{yz} orbitals (Δ and v in Figure 1) at the Fe(II) active site can be obtained through ligand field theory.[5] A strong axial distortion of an octahedron (i.e., contraction along the z axis) raises the energy of the d_{xz} and d_{yz} orbitals relative to the d_{xy} orbital, resulting in the $^5B_2$ state being lowest in energy (positive Δ in Figure 1). Second-order spin–orbit coupling of the $^5B_2$ with the ^5E excited state (in the C_{4v} complex) leads to the zero field splitting of the $^5B_2$ state such that the $M_s = 0$ component is lowest in energy, Figure 5, left, where now $D = \lambda^2/\Delta$ from ligand field theory and λ is the spin–orbit coupling constant for Fe(II) (≈ -80 cm^{-1}).[10] Therefore, a positive D corresponds to a positive value of Δ. However, for Fe(II) SOD and SBL, D is negative, which corresponds to a negative Δ in Figure 1 and therefore to a ^5E ground state, indicating that these systems have axially elongated C_{4v} sites. This is a more complex problem than had been generally realized since *the ^5E state has orbital as well as spin degeneracy and thus cannot be described by the usual spin-Hamiltonian formalism in eq 1.* We have evaluated the ligand field Hamiltonian given in eq 2, which includes spin–orbit (λ), axial (Δ), and rhombic (v) low-symmetry effects on the orbital as well as spin angular momentum of the $^5T_{2g}$ octahedral ground state in Figure 1. (Note that for a T_{2g} octahedral state the effective orbital angular momentum is $L = -1$, with M_L components corresponding to complex combinations of the d_{xy}, d_{xz}, and d_{yz} orbitals.) This produces the ground-state energy

$$\mathcal{H} = \lambda LS + \Delta(L_z^2 - (1/3)L(L+1)) + v(L_x^2 - L_y^2) \quad (2)$$

level diagram in Figure 6, which is very different from that obtained from the spin-Hamiltonian in Figure 5. A weak axial distortion of the site produces a ^5E ground state (in the C_{4v} complex) which is spin–orbit split into five equally spaced 2-fold degenerate levels. The lowest doublet is further split by a rhombic distortion of the site to give the δ measured in the temperature and field dependent MCD experiment.

We can now calculate δ and $g_\parallel$ (the latter is obtained by inclusion of the Zeeman term, $\beta(L_z + 2S_z)H$ in eq 2) in terms of the t_{2g} d orbital splittings, Δ and v, and these results are given in Figure 13 in ref 5b. A key point of this ligand field calculation is that large values of δ correspond to small values of $-\Delta$, while small values of δ require a large splitting of the d_{xy} orbital from the $d_{xz,yz}$ set which would result from the removal of one axial ligand on going to a five-coordinate weak axial structure. This ligand field model enables the experimental δ and $g_\parallel$ values in Table I obtained from the variable temperature, variable field MCD data to be used to estimate $-\Delta$ and v which define the $^5T_{2g}$ ground-state splitting in Figure 1. These values are also included in Table I. The octahedral Fe(II) model complex and Fe(II) SBL both show a small splitting (<500 cm^{-1}) of the $^5T_{2g}$ state consistent with the octahedral effective geometry for reduced lipoxygenase obtained from the excited-state Δ^5E_g splitting (vide supra), while the square pyramidal model and Fe(II) SOD show a large splitting (>1000 cm^{-1}) of the $^5T_{2g}$ ground state consistent with the large distortion associated with the vacant axial site in a five-coordinate structure. At this point, we have developed a protocol using Abs, CD, and low temperature MCD spectroscopies to define the excited-state splitting of the ^5E_g octahedral state and variable temperature, variable field MCD data to obtain the ground-state splittings of the $^5T_{2g}$ state. Thus we can *experimentally obtain the ligand field splitting of the d orbitals of the iron center (Figure 1) which probes the geometric and electronic structure of the Fe(II) active site.*

Molecular Mechanism of the Extradiol Dioxygenases: Metapyrocatechase

Metapyrocatechase (catechol 2,3-dioxygenase) catalyzes the extradiol ring cleavage of catechol with the insertion of both atoms of molecular oxygen to produce α-hydroxymuconic ϵ-semialdehyde. The Fe(II) site is active in catalysis which involves an ordered bi-uni mechanism where the binding of substrate is required for O_2 reactivity. This enzyme system, investigated in collaboration with Professor J. Lipscomb,[11] provides an important application of the above excited-state spectroscopic protocol to the study of a non-heme Fe(II) center and its interactions with substrate and small molecules which are of direct relevance to the catalytic mechanism.

The near-IR CD/MCD spectra of metapyrocatechase show ligand field transitions at 5220 and 11 240 cm^{-1}; therefore, Δ^5E_g is $\sim$6000 cm^{-1} and thus the effective site structure is square pyramidal. Analogous to the variable temperature, variable field MCD data on Fe(II) SOD presented in Figure 4, the saturation magnetization curves of metapyrocatechase are nested and described by the non-Kramers doublet model in Figure 5 with $\delta = 4$ cm^{-1} and $g_\parallel = 8.9$, which give values of $-\Delta$ and v in Figure 1 of 600 and 300 cm^{-1}, respectively. Addition of N_3^- produces no change in energy or saturation magnetization behavior of the ligand field transitions, indicating that this small molecule does not bind to the resting Fe(II) active site. In contrast, anaerobic addition of the catechol substrate causes a large increase in Δ^5E_g and a significant change in the saturation behavior, indicating that the ground-state $^5T_{2g}$ splitting also has increased. Mössbauer studies on this system showed no change in the Fe(II) site with substrate addition;[12] the MCD results in ref 11, in fact, provide the

(10) Reduced from the free ion value of ~ -100 cm^{-1} due to covalency.

(11) Mabrouk, P. A.; Orville, A. M.; Lipscomb, J. D.; Solomon, E. I. *J. Am. Chem. Soc.* **1991**, *113*, 4053–4061.

(12) Tatsuno, Y.; Saeki, Y.; Nozaki, M.; Otsuka, S.; Maeda, Y. *FEBS Lett.* **1983**, *112*, 83.

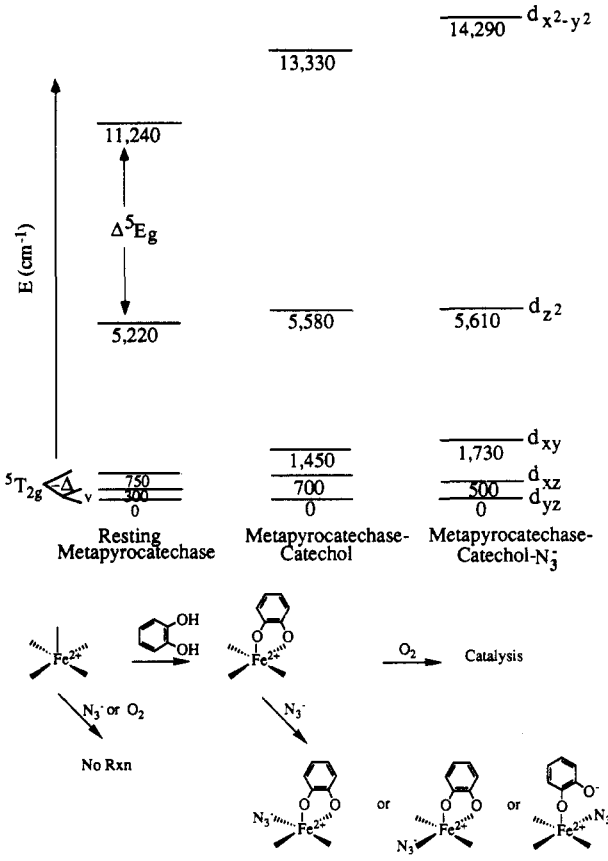

Figure 7. Experimental d orbital energy level diagram for resting metapyrocatechase, its substrate complex, and the enzyme–substrate–azide ternary system (top). Spectroscopically effective structural mechanism derived from this energy diagram for the Fe(II) active site in metapyrocatechase (bottom).

first evidence for substrate binding to this Fe(II) active site. Further, addition of N_3^- in the presence of substrate causes an additional increase in Δ^5E_g and change in the saturation behavior demonstrating that *substrate binding activates this active site for small molecule binding.* It should be emphasized that substrate binding is also required for O_2 reactivity.

The data on metapyrocatechase and the analysis described above allow one to construct an experimentally derived ligand field energy level diagram of the d orbital splittings which probes the geometric and electronic structure of this Fe(II) active site and its change with substrate and small molecule binding (Figure 7).[11] In particular, it is found that the square pyramidal splitting of the d orbitals of resting Fe(II) metapyrocatechase changes with catechol binding such that the $d_{x^2-y^2}$ and d_{xy} levels increase in energy. Since catechol is a weak field ligand for Fe(II), the change in energy of these orbitals indicates that the catechol binds at the axial position, allowing the iron to move into the plane of the equatorial ligands. The d_{xz}–d_{yz} splitting also increases, indicating that the catechol binds in a bidentate fashion with the second oxygen coordinating in the equatorial plane. This is consistent with results based on isotopically labeled substrate binding to the EPR active NO complex of this enzyme.[13] The further shift in the d orbital energies with N_3^- addition in Figure 7 indicates that catechol binding labilizes the active site for equatorial small molecule binding. There

(13) Arciero, D. M.; Lipscomb, J. D. *J. Biol. Chem.* **1986**, *261*, 2170.

Scheme I

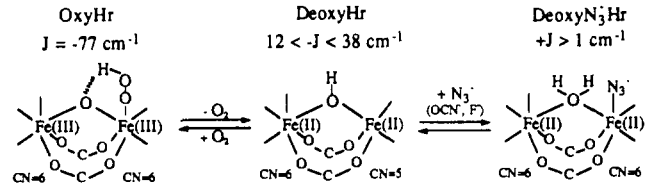

appear to be both geometric and electronic contributions to this activation. Substrate coordination results in a distortion of the site such that the Fe(II) center moves into the equatorial plane, which produces a large splitting of the t_{2g} set of d orbitals, localizing the extra electron of the Fe(II) in the lowest energy d_{yz} orbital oriented along one equatorial ligand–metal axis. This anisotropic electron density will weaken the bonding interaction of the Fe(II) with a donor ligand in the equatorial plane and activate this ligand's position for reactivity with an electron acceptor small molecule, in particular, the dioxygen involved in catalysis. These excited-state studies have provided significant insight into the active site of metapyrocatechase and establish the utility of this spectroscopic protocol in obtaining molecular level insight into catalytic processes in non-heme Fe(II) enzymes.

Spectroscopic Effects of Dimer Interactions: Deoxyhemerythrin

We now turn to the binuclear non-heme proteins and consider the additional spectral consequences associated with a dimer site. These include excited-state contributions from both Fe(II) centers and the possibility of electronic coupling between the two Fe(II) centers, which can strongly affect the ground-state properties. We first focus on hemerythrin (Hr), which is the best characterized of these proteins. DeoxyHr has a binuclear Fe(II) active site, [$Fe^{II}Fe^{II}$], which reversibly binds dioxygen to form oxyHr. OxyHr is generally accepted to have two six-coordinate ferric centers, [$Fe^{III}Fe^{III}$], bridged by two carboxylates and an oxo group.[14,15] The dioxygen is reduced by 2 equiv and binds to one iron[16] as hydroperoxide, which is thought to be hydrogen bonded to the μ-oxo group (Scheme I).[17] The excited-state spectral studies described below provided the first detailed geometric and electronic structural insight into the deoxyHr site and its interactions with small molecules, and it provides a basis for the structure/function correlations to other binuclear Fe(II) enzymes described in the next section. These studies define the ligation and coordination unsaturation of each iron and the nature of the bridging ligands at the binuclear Fe(II) site. It should be noted that for oxyHr (and metHr) the original model of an oxo bridge came mostly from

(14) Crystal structures have been reported for both the metHr and met N_3^- Hr derivatives. Met contains one five- and one six-coordinate Fe(III) bridged by an oxo and two carboxylates; the five-coordinate Fe(III) binds exogenous ligands, which results in two six-coordinate Fe(III) centers in met N_3^-. Holmes, M. A.; Stenkamp, R. E. *J. Mol. Biol.* **1991**, *220*, 723–737.

(15) (a) Magnetic susceptibility: Dawson, J. W.; Gray, H. B.; Hoenig, H. E.; Rossman, G. R.; Schredder, J. M.; Wang, R. H. *Biochemistry* **1972**, *11*, 461–465. (b) Mössbauer: Garbett, K.; Johnson, C. E.; Klotz, I. M.; Okamura, M. Y.; Williams, R. J. P. *Arch. Biochem. Biophys.* **1971**, *142*, 574–583. (c) Raman: Dunn, J. B. R.; Shriver, D. F.; Klotz, I. M. *Proc. Natl. Acad. Sci. U.S.A.* **1973**, *70*(9), 1582–2584.

(16) Gay, R. R.; Solomon, E. I. *J. Am. Chem. Soc.* **1978**, *100*, 1972–1973.

(17) Shiemke, A. K.; Loehr, T. M.; Sanders-Loehr, J. *J. Am. Chem. Soc.* **1986**, *108*(9), 2437–2443.

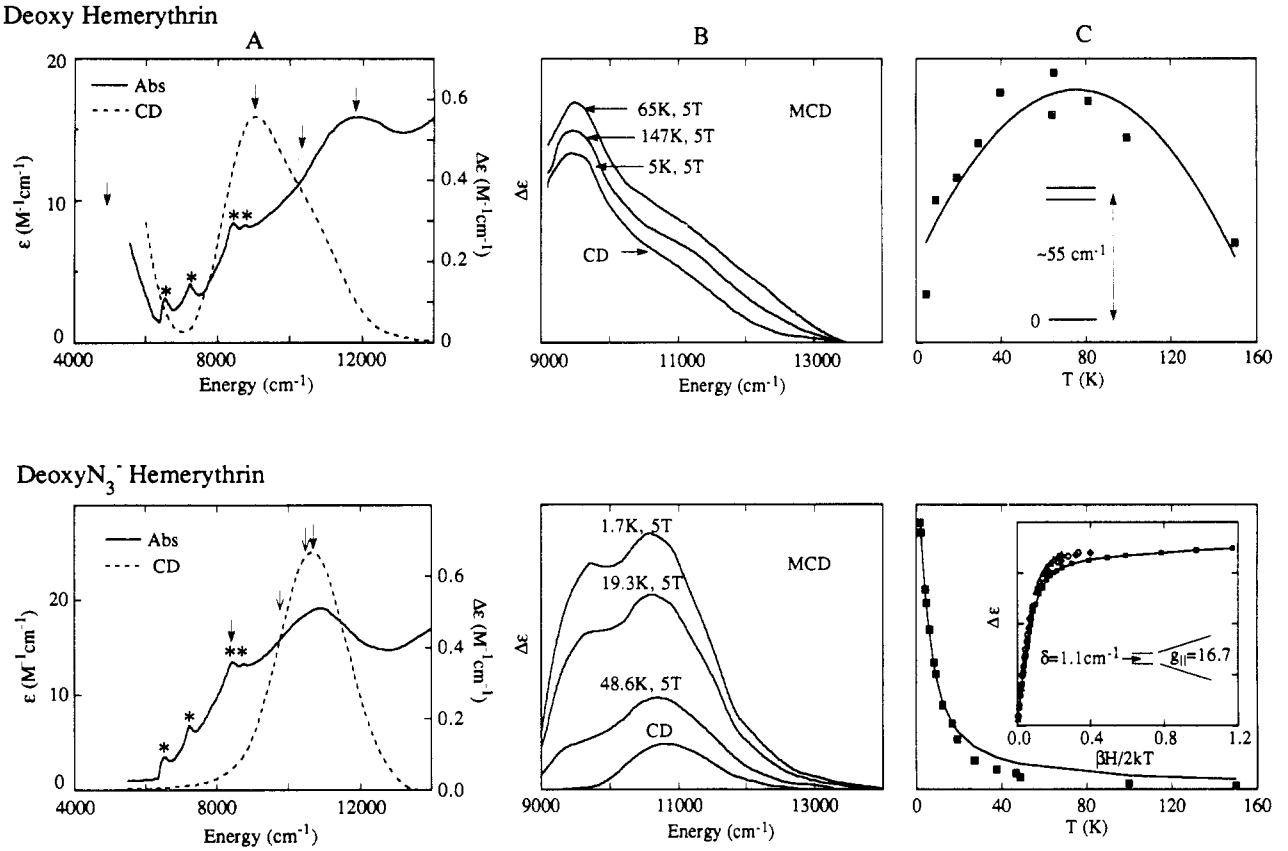

Figure 8. Abs, CD, and MCD spectra of deoxyHr (top) and deoxy N_3^- Hr (bottom). (A) Room temperature Abs (—) and CD (- - -) spectra. Arrows indicate approximate positions of the ligand field transitions (open arrows are from the MCD data shown in B), and the sharp absorbance features (*) arise from the vibrational background. (B) Variable temperature MCD spectra of the ligand field transitions at a fixed magnetic field (5 T). (C) Temperature dependence of the MCD intensity in B. The solid line in C-top was obtained from the energy level diagram included in this frame.[18b] Saturation magnetization curves for deoxy N_3^- Hr are given in the inset of C-bottom. The solid line fit to the data points gives the non-Kramers doublet spitting included in this frame.

magnetic susceptibility studies,[15a] which determined that this site was strongly antiferromagnetically coupled ($J = 77$ cm^{-1} for $\mathcal{H} = -2JS_1S_2$, where S_1 and S_2 are the total spins on each iron center). The large magnitude of the exchange coupling parameter, J, requires a very effective superexchange pathway and thus a quite covalent (i.e., oxo) bridging ligand. The effects on this oxo bridge of reduction and of exogenous ligand binding to the deoxyHr site can also be probed by the determination of the exchange coupling through its effects on the ground-state magnetic properties of these binuclear Fe(II) sites as described below.

A combination of near-IR Abs and CD data shows[18] that deoxyHr exhibits three ligand field transitions in the ~10 000-cm^{-1} region and a fourth transition at ~5000 cm^{-1} (arrows in Figure 8A). Only N_3^-, OCN^-, and F^- are found to bind to the deoxyHr site. As shown for deoxy N_3^- Hr in Figure 8A, this binding eliminates the 5000-cm^{-1} band. Thus the deoxyHr site has one six- and one five-coordinate iron, the latter being unsaturated and binding the small molecule, which results in two six-coordinate Fe(II) centers.

The temperature and field dependent MCD data for deoxyHr and deoxy N_3^- Hr are strikingly different from the data obtained for the mononuclear Fe(II) enzymes described thus far in this Account. As shown in Figure 8B for the higher energy ligand field region, *deoxyHr at low temperature and high magnetic field exhibits no MCD signal.* An MCD signal appears and increases in intensity as the temperature is increased for fixed magnetic field, maximizes at ~70 K, and then decreases to higher temperature. These data are plotted in Figure 8C, which shows that an MCD inactive singlet state must be the lowest energy component of the ground state with an MCD active "doublet" set of levels thermally accessible at ~55 cm^{-1}. For deoxy N_3^- Hr a large MCD signal is observed at low temperature which decreases as the temperature increases. This behavior (Figure 8C) parallels the data on the mononuclear Fe(II) centers described earlier which have MCD active non-Kramers $M_s = \pm 2$ doublets lowest in energy. However, the saturation magnetization data for deoxy N_3^- Hr (inset in Figure 8C) are fit by a non-Kramers spin-Hamiltonian model with $\delta \approx 1$ cm^{-1} and $g_\parallel \approx 17$, which is far larger than the $g_\parallel \sim 8$ associated with the ± 2 doublet of a mononuclear Fe(II) center.

We have applied the spin-Hamiltonian in eq 3 to describe the ground state of these binuclear Fe(II) sites ($S_1 = 2$, $S_2 = 2$), where the first term (in J) allows for exchange coupling between the Fe(II) centers, and the remaining two terms (in D) allow for the zero field splitting (ZFS) of each mononuclear Fe(II) center.

$$\mathcal{H} = -2J(S_1S_2) + D_1[(S_{z_1})^2 - (1/3)S_1(S_1 + 1)] + D_2[(S_{z_2})^2 - (1/3)S_2(S_2 + 1)] \quad (3)$$

Depending on the relative magnitudes of J, D_1, and D_2 (and rhombic splittings on each iron center; see ref 18b),

(18) (a) Reem, R. C.; Solomon, E. I. *J. Am. Chem. Soc.* **1984**, *106*, 8323–8325. (b) Reem, R. C.; Solomon, E. I. *J. Am. Chem. Soc.* **1987**, *109*, 1216–1226.

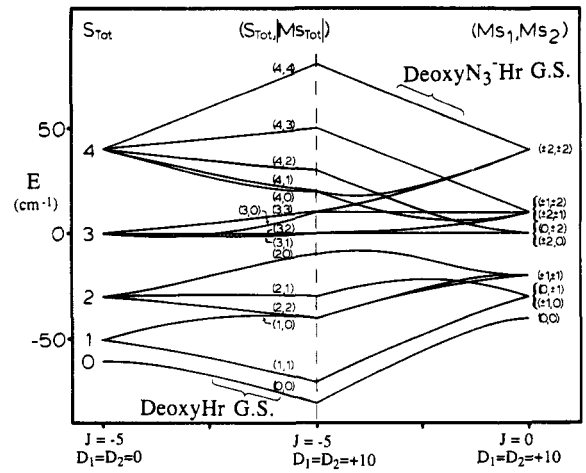

Figure 9. Correlation diagram of the energy levels of binuclear Fe(II) ground state including exchange coupling and single-site ZFS. The left side is the limit of only antiferromagnetic coupling between two $S = 2$ ions which gives states designated by the total spin of the dimer S_{total}. The right side gives the pure ZFS limit (positive, axial for both ions) with states designated by the M_s value of each Fe(II) center (M_{s1}, M_{s2}). The central portion shows the splittings when both ZFS and exchange coupling are present with states labeled as coupled wavefunctions ($S_{total}|M_{s\,total}|$). Note that while this diagram has assumed specific values for J, D_1, and D_2 in eq 3, it describes the general behavior predicted for two antiferromagnetically coupled Fe(II) ions each with positive ZFS and can be used to describe a system with ferromagnetic coupling between two Fe(II) ions each with negative ZFS by reversing the energy scale such that the (4,4) energy level becomes the ground state. Additional diagrams for different combinations of J, D_1, D_2, and E are available in ref 18b.

eq 3 leads to energy level diagrams[19] such as the one in Figure 9. The right-hand side corresponds to the zero exchange coupling limit while the left-hand side assumes no ZFS. The temperature and field dependent MCD data and ground-state splittings given in Figure 8C for deoxyHr could be fit using the right-hand side of this diagram if one assumes no exchange coupling and positive ZFS on each Fe(II) center. In this limit an MCD inactive $M_s = 0$ is lowest on each Fe(II) center and an $M_s = \pm 1$ MCD active doublet is the first excited state. However, this would require values of the Fe(II) ZFS parameter D of ~ 35 cm^{-1}, which is far larger than the maximum value of ~ 15 cm^{-1}.[20] Alternatively, one can fit the data for deoxyHr in Figure 8C using the pure exchange coupling limit on the left in Figure 9. In this limit two $S = 2$ ions are antiferromagnetically coupled to produce an $S_{total} = 0$ MCD inactive singlet ground state with an MCD active $S_{total} = 1$ excited state at $2J$, which would give a J value of ~ 25 cm^{-1}. However, the Fe(II) ZFS must have a value comparable to this fairly low exchange coupling, and thus both effects must be included in a quantitative fit of the deoxyHr and deoxy N_3^- Hr data (center of Figure 9).

The position on this diagram appropriate for deoxyHr is indicated at the bottom of Figure 9, which gives an antiferromagnetically coupled ground state with the value of J dependent on the value of D. This imposes limits on the exchange coupling in deoxyHr of $12 < -J < 38$ cm^{-1}. The lower limit of 12 cm^{-1} is too large an antiferromagnetic coupling for only carboxylate bridges[21] and indicates that deoxyHr must have an additional bridging ligand derived from the oxo group. Since for the same structure and bridging ligation the J for a binuclear Fe(II) site should be larger than for a binuclear Fe(III) site ($J_{Fe(II)} \sim (25/16)J_{Fe(III)}$ from eq 7, ref 18b), the upper limit on the antiferromagnetic coupling of 38 cm^{-1} appeared to be too small for an oxo bridge, which led to the model[18] that deoxyHr has a hydroxide bridge as indicated in Scheme I.[22]

For deoxy N_3^- Hr, the data in Figure 8C indicate that the ground state is an MCD active *non-Kramers doublet with a $g_{\|} \sim 16$, which led us to conclude that the two Fe(II) centers in this site were weakly ferromagnetically coupled.*[18] This corresponds to a positive value of J, which reverses the energy scale in Figure 9 to produce the ground state for deoxy N_3^- Hr indicated at the top right, which corresponds to ferromagnetic coupling of two $S = 2$ ions, each with negative single site ZFS such that their $M_s = \pm 2$ are lowest. It should be noted that in our original study of this system we placed a lower limit on the weak ferromagnetic coupling of $J > 1$ cm^{-1}. More recent studies[23] indicate a value of ~ 2 cm^{-1}.

As shown in Scheme I, loss of dioxygen leads to reduction of oxyHr to the binuclear Fe(II) deoxy state, which raises the pK_a and leads to protonation of the μ-oxo to form an OH$^-$ bridge. The binding of certain ligands at the open coordination position of the five-coordinate Fe(II) center of deoxyHr leads to a dramatic reduction of the exchange coupling and a weakly ferromagnetic site. Thus the azide appears to inductively raise the pK_a of the OH$^-$ bridge leading to its protonation either forming a water bridge or disrupting the bridge entirely. Either possibility would be consistent with the weak ferromagnetic coupling; however, we favor[18] the water-bridging model due to the fact that both irons of deoxy N_3^- Hr are six-coordinate in a sterically crowded site.[14] Scheme I provides structural insight into earlier observations[24] that solvent water exchanges rapidly with the oxo bridge only in the reduced state and then only in the presence of N_3^- or OCN$^-$, as water bound to transition metal complexes exchanges ~ 3 orders of magnitude faster than hydroxide.[25] The oxo–hydroxo equilibrium in Scheme I should also contribute to the reversible binding of dioxygen by this site. As will be discussed in the last section of this Account, oxidation of deoxyHr to the met level by one-electron oxidants is slow, while the two-electron oxidation upon binding dioxygen is rapid. The latter could result from facile proton transfer from the bridging hydroxide directly to the bound dioxygen molecule to form the oxo bridge. Finally this deprotonation of the bridge may

(19) Note that this treatment is approximate as it has not allowed for the orbital contributions to the zero field splitting described in Figure 6 for the case of negative D.

(20) Champion, P. M.; Sievers, A. *J. Chem. Phys.* **1977**, *66*, 1819–1825.

(21) Cheng, C.; Reiff, W. M. *Inorg. Chem.* **1977**, *16*, 2097–2103.

(22) More recently, Wieghardt has prepared a binuclear Fe(II) model complex with an OH$^-$ bridge which exhibits a similar exchange coupling to deoxyHr. Also crystallographic and EXAFS data on deoxyHr support this model. (a) Hartman, J. R.; Rardin, R. L.; Chaudhuri, P.; Pohl, K.; Wieghardt, K.; Nuber, B.; Weiss, J.; Papaefthymiou, G. C.; Frankel, R. B.; Lippard, S. *J. Am. Chem. Soc.* **1987**, *109*, 7387–7396. (b) Holmes, M. A.; Trong, I. L.; Turley, S.; Sieker, L. C.; Stenkamp, R. E. *J. Mol. Biol.* **1991**, *218*, 583–593. (c) Zhang, K.; Stern, E. A.; Ellis, F.; Sanders-Loehr, J.; Shiemke, A. K. *Biochemistry* **1988**, *27*, 7470–7479.

(23) (a) Hendrich, M. P.; Pearce, L. L.; Que, L.; Chasteen, N. D.; Day, E. P. *J. Am. Chem. Soc.* **1991**, *113*, 3039–3044. (b) McCormick, J. M.; Pulver, S.; Solomon, E. I. Unpublished results.

(24) Freier, S. M.; Duff, L. L.; Shriver, D. F.; Klotz, I. M. *Arch. Biochem. Biophys.* **1980**, *205*, 449.

(25) Basolo, F.; Pearson, R. B. *Mechanisms of Inorganic Reactions*; Wiley: New York, 1967; p 165.

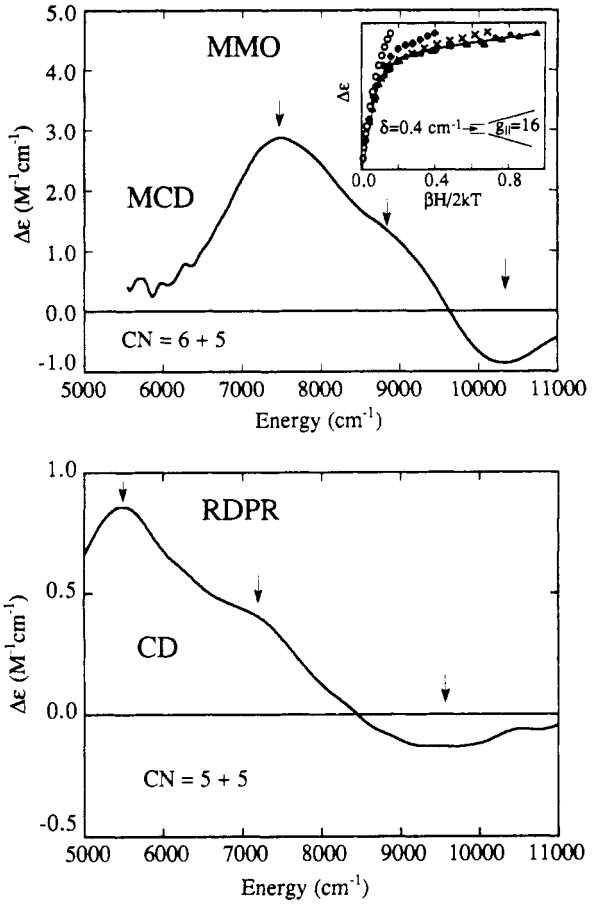

Figure 10. Top: Low-temperature MCD spectrum of fully reduced MMO. Inset: Saturation magnetization curves giving the non-Kramers doublet splitting parameters indicated. Bottom: CD spectrum of fully reduced RDPR. Arrows in both spectra indicate approximate positions of ligand field transitions which give the coordination number (CN) of each iron center.

play a role in the structural constraint which regulates the redox potential of this site and is responsible for the cooperativity in oxygen binding which we have shown to be present in the Hr from the brachiopod *Lingula reevii* as described in ref 26.

Structure/Function Correlations: Reduced Methane Monooxygenase and Ribonucleotide Reductase

While deoxyHr reversibly binds dioxygen as peroxide at one iron center, fully reduced, [$Fe^{II}Fe^{II}$], methane monooxygenase (MMO) activates dioxygen for hydroxylation of saturated and unsaturated hydrocarbons,[27] and reduced ribonucleotide diphosphate reductase (RDPR) reduces dioxygen and generates a tyrosine radical which is active in catalysis.[28] Near-IR CD/MCD studies define variations among these active sites which provide insight into differences in their dioxygen reactivity. Our studies on MMO are being performed in collaboration with Professor J. Lipscomb,[29] and those on RDPR are in collaboration with

Scheme II

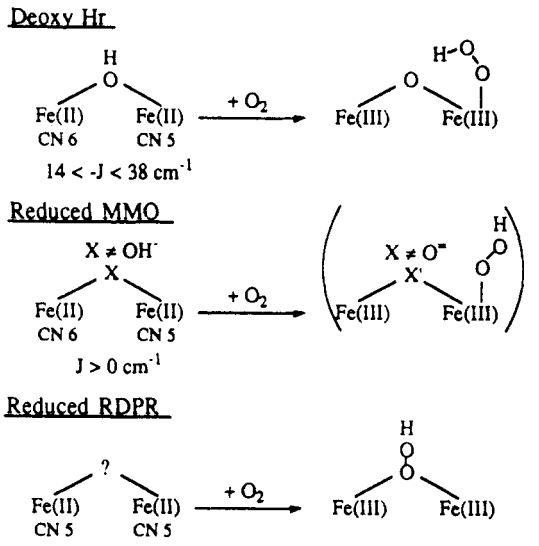

Professor J. Stubbe.[30] From the low-temperature MCD spectrum of reduced MMO in Figure 10 there is one ligand field transition at 7400 cm^{-1} which is too low in energy for a six-coordinate Fe(II) center, indicating that, as with deoxyHr, reduced MMO has an open coordination position at one iron of the binuclear site. However, in contrast to deoxyHr, which is not MCD active at low temperature, reduced MMO exhibits a large MCD signal at low temperature which has a saturation magnetization behavior indicating that there is a non-Kramers doublet lowest in energy which has $g_{\parallel} \sim 16$ (inset, Figure 10). Thus the site is weakly ferromagnetically coupled, consistent with the results of Lipscomb and Münck.[31] This indicates that *the hydroxide bridge responsible for the antiferromagnetism of deoxyHr is not likely to be present in the reduced MMO site* (Scheme II). EXAFS studies on oxidized, [Fe^{III}-Fe^{III}], MMO indicate that the oxo bridge of met- and oxyHr is also not present at this oxidation level in this enzyme.[32] This variation in the key bridging ligand would appear to play an important role in the difference in O_2 reactivity of these sites perhaps by destabilizing the proposed peroxide level intermediate at a single iron center in MMO as in Scheme II.

The near-IR CD spectrum[30] of reduced RDPR in Figure 10 is strikingly different from that of deoxyHr and reduced MMO in that it exhibits two low-energy ligand field transitions (at 5480 and 7000 cm^{-1}) indicating that both irons are five-coordinate or less. Thus *in contrast to deoxyHr and reduced MMO, both irons in reduced RDPR appear to have open coordination positions for O_2 reactivity.* This raises the interesting possibility that the peroxide level intermediate reported by Stubbe et al.[33] could be bridging between the two ferric centers. As indicated in Scheme II, we would favor this to involve a μ-1,1 hydroperoxide, on the basis of our results on the peroxide intermediate at the tri-

(26) (a) Richardson, D. E.; Reem, R. C.; Solomon, E. I. *J. Am. Chem. Soc.* **1983**, *105*, 7780–7781. (b) Richardson, D. E.; Emad, M.; Reem, R. C.; Solomon, E. I. *Biochemistry* **1987**, *26*, 1003.

(27) (a) Fox, B. G.; Froland, W. A.; Dege, J. E.; Lipscomb, J. D. *J. Biol. Chem.* **1989**, *264*(17), 10023–10033. (b) Woodland, M. P.; Dalton, H. *J. Biol. Chem.* **1984**, *259*(1), 53–39.

(28) Thelander, L.; Larsson, B.; Hobbs, J.; Eckstein, F. *J. Biol. Chem.* **1976**, *251*(5), 1398–1405.

(29) Pulver, S.; Fox, B.; Froland, W.; Lipscomb, J.; Solomon, E. Unpublished results.

(30) McCormick, J. M.; Reem, R. C.; Foroughi, J.; Bollinger, J. M.; Jensen, G. M.; Stephens, P. J.; Stubbe, J.; Solomon, E. I. *New J. Chem.* **1991**, *15*, 439–444.

(31) Hendrich, M. P.; Münck, E.; Fox, B. G.; Lipscomb, J. D. *J. Am. Chem. Soc.* **1990**, *112*, 5861.

(32) DeWitt, J. G.; Bentsen, J. G.; Rosenzweig, A. C.; Hedman, B.; Green, J.; Pilkington, S.; Papaefthymiou, G. C.; Dalton, H.; Hodgson, K. O.; Lippard, S. J. *J. Am. Chem. Soc.* **1991**, *113*, 9219–9235.

(33) Bollinger, J. M.; Edmondson, D. E.; Huynh, B. H.; Filley, J.; Norton, J.; Stubbe, J. *Science* **1991**, *253*, 292.

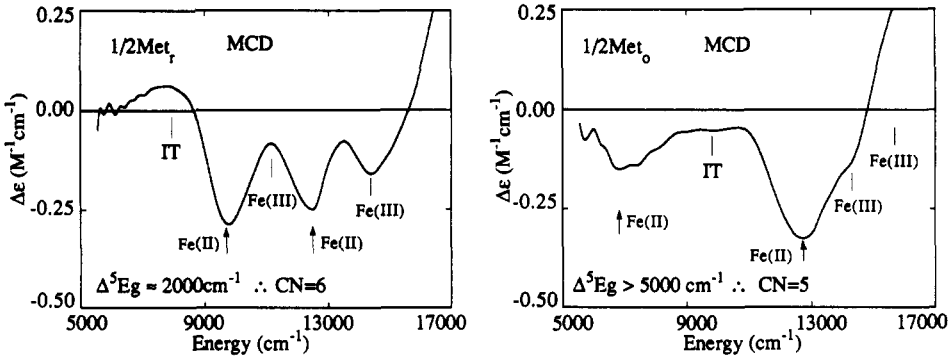

Figure 11. Low-temperature MCD spectra of half-met$_r$ (left) and half-met$_o$ (right) hemerythrin. Arrows indicate the ligand field transitions of the Fe(II) center giving Δ^5E_g values and thus the coordination of the Fe(II) center. The lines indicate the positions of the intervalence transfer transition (IT) and the spin-forbidden ligand field transitions of the ferric center (Fe(III)), respectively. See ref 36.

Scheme III

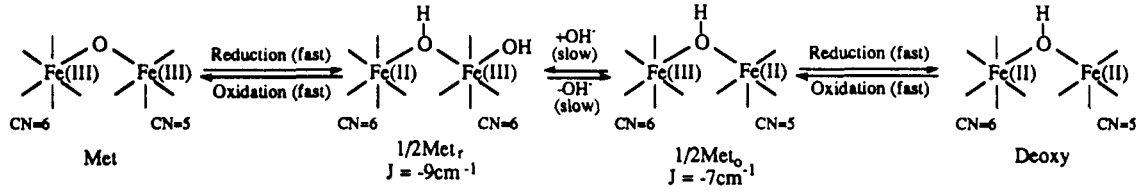

nuclear copper site of the multicopper oxidases.[34]

Mixed-Valent, [$Fe^{II}Fe^{III}$], Active Sites: One-Electron Redox Chemistry of Hemerythrin

Hemerythrin exhibits some very unusual one-electron redox chemistry involving the mixed-valent, half-met (or semi-met) derivative.[35] DeoxyHr, [$Fe^{II}Fe^{II}$], is oxidized by one electron to produce the half-met$_o$ derivative, which is rapidly reduced but has a lower rate for further oxidation. One-electron reduction of the metHr, [$Fe^{III}Fe^{III}$], produces the half-met$_r$ derivative, which has a very different EPR signal from that of half-met$_o$ and is quickly reoxidized but slow to further reduce. The excited-state spectral protocol presented above has been applied to these mixed-valent sites and provides electronic and geometric structural insight into the differences in half-met$_r$ and half-met$_o$ which relate to their different redox chemistry.[36]

The half-met derivatives involve one Fe(II) with $S = 2$ which is antiferromagnetically coupled to an Fe(III) with $S = {}^5/_2$ to produce an $S_{total} = {}^1/_2$ ground state from EPR studies.[35] The low-temperature MCD spectrum of this derivative will be dominated by the ligand field transitions of the Fe(II) center as the ligand field bands of Fe(III) are spin forbidden and therefore weak while the intervalence transfer (IT) transition, which is present in these mixed valent sites and fairly intense in Abs, makes very little contribution to the low-temperature MCD spectrum due to the C-term selection rule.[37] From Figure 11, half-met$_r$ exhibits two intense Fe(II) ligand field transitions at 9800 and 12200 cm^{-1}. Thus Δ^5E_g is ~2000 cm^{-1} and the Fe(II) center is six-coordinate. In contrast, the Fe(II) center in the half-met$_o$ exhibits one intense ligand field transition at 12600 cm^{-1}. The lack of a second band at ~10000 cm^{-1} requires that this Fe(II) is less than six-coordinate. As a five-coordinate Fe(II) should have a band ~5000 cm^{-1} below the 12600-cm^{-1} band, the other intense feature at ~7100 cm^{-1} in the half-met$_o$ spectrum can be assigned as the second ligand field transition of a five-coordinate Fe(II).

Variable temperature, variable field MCD studies have been performed[36] on both half-met sites and analyzed in terms of exchange and ZFS as in eq 3 to obtain values for the exchange coupling constant, J, of −9 cm^{-1} for half-met$_r$ and −7 cm^{-1} for half-met$_o$.[38] Thus both sites have similar antiferromagnetic pathways, and the magnitude of J is consistent with a bridging hydroxide as has been suggested for half-met N_3^-.[39] Finally, we have found that half-met$_r$ and half-met$_o$ are in a pH equilibrium with half-met$_r$ being the high pH form. Since there is no change in the bridging ligand, *this pH conversion of half-met$_o$ to half-met$_r$ must involve exogenous OH^- binding to the open coordination position present at the Fe(II) center in half-met$_o$.* Note from Scheme III that OH^- binding induces an intramolecular shift of the extra electron to the adjacent iron.[35c,40]

The spectroscopically effective active site models in Scheme III provide structural insight into the redox chemistry of this protein site. Methemerythrin has one five- and one six-coordinate Fe(III) which are bridged by an oxo group.[14a] Reduction to half-met$_r$ would involve H_2O simultaneously protonating the bridge and binding as exogenous hydroxide. Slow loss of the ex-

(34) Cole, J. L.; Ballou, D. P.; Solomon, E. I. *J. Am. Chem. Soc.* **1991**, *113*, 8544.

(35) (a) Wilkins, R. G.; Harrington, P. C. The Chemistry of Hemerythrin. In *Advances in Inorganic Biochemistry* Theil, E. C., Eichhorn, G. L., Marzilli, L. G., Eds.; Elsevier: New York, 1983; Vol. 5, pp 51–85. (b) Armstrong, G. D.; Ramasami, T.; Sykes, A. G. *J. Chem. Soc., Chem. Commun.* **1981**, 1017–1019. (c) Pearce, L. L.; Kurtz, D. M., Jr.; Xia, Y. M.; Debrunner, P. G. *J. Am. Chem. Soc.* **1987**, *109*, 7286–7293.

(36) (a) McCormick, J. M.; Solomon, E. I. *J. Am. Chem. Soc.* **1991**, *112*, 2005. (b) McCormick, J. M.; Reem, R. C.; Solomon, E. I. *J. Am. Chem. Soc.* **1991**, *113*, 9066.

(37) This derives from the fact that low-temperature MCD intensity requires two perpendicular transition moments while an IT transition involves optical excitation of an electron from the Fe(II) to the Fe(III) and thus is unidirectional.

(38) This involves energy level diagrams equivalent to that in Figure 9 for exchange coupling of an $S = {}^5/_2$ with a zero-field-split $S = 2$ center. These are presented in ref 36b.

(39) Maroney, M. J.; Kurtz, D. M.; Nocek, J. M.; Pearce, L. L.; Que, L. *J. Am. Chem. Soc.* **1986**, *108*, 6871–6879.

(40) The structural model of OH^- binding to the Fe(III) in half-met$_r$ derives from spectral studies on a series of half-met L derivatives[36b] which demonstrate that the exogenous ligand, L, binds to the Fe(III).

ogenous OH^- produces half-met$_o$ with one five- and one six-coordinate iron which are still hydroxo bridged. This is structurally equivalent to the deoxy site described in Scheme I. Thus there should be a very low Franck-Condon barrier for the one-electron interconversion between these forms of the hemerythrin active site.

Concluding Remarks

At this point a powerful excited-state spectroscopic methodology has been developed to probe non-heme Fe(II) active sites. It has provided important molecular level insight into the mechanism of the extradiol dioxygenases and the chemistry of hemerythrin, and it is defining structure/function correlations over the coupled binuclear non-heme iron proteins. Our research efforts are now evolving in a number of complementary directions. We are further developing this spectroscopic protocol and extending it to other non-heme Fe(II) enzymes and their interactions with substrate, small molecules, and cofactors of relevance to catalysis. Systems presently being studied include bleomycin, phenylalanine hydroxylase,[41] methane monooxygenase, ribonucleotide reductase, and acid phosphatase, the latter being active in catalysis in its mixed-valent state.[42] We are also extending our spectroscopic studies on non-heme ferrous enzymes to define oxygen analogues and intermediates. Many of these proteins form reversible complexes with NO. These $\{FeNO\}^7$ complexes have quite unusual spectral features, including an $S = {}^3/_2$ ground state.[43] These spectral features appear to relate to spin polarization effects,[44] and once understood they should allow one to probe for variations in electron delocalization over the $\{FeNO\}^7$ unit which would contribute to differences in O_2 activation by non-heme Fe(II) sites. Finally, in addition to the stable oxyhemerythrin site, oxygen intermediates have been reported for bleomycin[45] and ribonucleotide reductase.[33] Spectroscopic studies combined with self-consistent field-Xα-scattered wave calculations are presently being pursued on these and related systems to define electronic structure and how this is affected by geometric structural changes of relevance to catalysis.

This research has been supported by the NIH (GM40392 for the mononuclear non-heme iron enzyme studies) and the NSF (DMB-9019752 for the coupled binuclear non-heme iron protein studies). E.I.S. expresses his sincere appreciation to all his students and collaborators who are listed as coauthors in the literature cited for their commitment and major contributions to this science. We thank Sabine Pulver for her valuable assistance in the preparation of this manuscript.

(41) Yeager, M.; Glasfeld, E.; Caradonna, J.; Solomon, E. I. Unpublished results.

(42) (a) Vincent, J. B.; Olivier-Lilley, G. L.; Averill, B. A. *Chem. Rev.* **1990**, *90*, 1447-1467. (b) Antanaitis, B. C.; Aisen, P.; Lilienthal, H. R. *J. Biol. Chem.* **1983**, *258*, 3166-3172.

(43) (a) Galpin, J. R.; Veldink, G. A.; Vliegenthart, J. F. G.; Boldingh, J. *Biochim. Biophys. Acta* **1978**, *536*, 356-362. (b) Twilfer, H.; Bernhardt, F.-H.; Gersonde, K. *Eur. J. Biochem.* **1985**, *147*, 171. (c) Chen, V. J.; Orville, A. M.; Harpel, M. R.; Frolik, C. A.; Surerus, K. K.; Münck, E.; Lipscomb, J. D. *J. Biol. Chem.* **1989**, *264*, 21677. (d) Nocek, J. M.; Kurtz, D. M. *Biochemistry* **1988**, *27*, 1014-1024.

(44) Zhang, Y.; Pavlosky, M.; Brown, C.; Westre, T.; Solomon, E. I. Unpublished results.

(45) Burger, R. M.; Kent, T. A.; Horwitz, S. B.; Münck, E.; Peisach, J. *J. Biol. Chem.* **1983**, *258*, 1559.

Charge as a Key Component in Reaction Design. The Invention of Cationic Cyclization Reactions of Importance in Synthesis

LARRY E. OVERMAN

Department of Chemistry, University of California, Irvine, California 92717

Received February 19, 1992

It has been only within the last few decades that reactions of value in chemical synthesis have been created from scratch, rather than being discovered more or less by accident.[1,2] This Account will illustrate a feature of reaction design, the incorporation of a charged atom, that we have found to be particularly beneficial in the invention of new carbon-carbon bond-forming cyclization reactions. Our studies are founded on the observation that introduction of a charged atom into an array of atoms undergoing bond reorganization typically lowers the free energy of activation of the process. Thus, reactions of charged species typically occur under mild conditions where high selectivity in bond formation, a hallmark of useful reactions, is most probable.[3,4] The transformations that are the subject of this brief Account are depicted in Figure 1.

Larry E. Overman was born in Chicago, Illinois, in 1943. He obtained a B.A. degree from Earlham College in 1965 and completed his doctoral study in 1969 with Professor Howard W. Whitlock, Jr. at the University of Wisconsin. After working with Professor Ronald Breslow at Columbia University on an NIH postdoctoral fellowship, he joined the faculty at the University of California at Irvine in 1971. He is now Professor of Chemistry at Irvine and currently Chairman of the Department. Professor Overman's research interests focus on the invention of new reactions and strategies in organic synthesis and the total synthesis of complex target molecules.

(1) The state-of-the-art in organic synthesis has recently been reviewed in detail: *Comprehensive Organic Synthesis*; Trost, B. M., Fleming, I., Eds.; Pergamon Press: Oxford, 1991; Vols. 1-9.

(2) For one leading chemist's account of reaction invention, see: Barton, D. H. R. *Aldrichchim. Acta* **1990**, *23*, 3.

(3) Selectivity of a variety of types is desired. Positional (regioselectivity) and stereochemical (stereoselectivity and enantioselectivity) orientation and functional group selectivity (chemoselectivity) are of paramount importance.

(4) For discussion of reaction temperature and selectivity relationships, see: (a) Seebach, D.; Hidber, A. *Chimia* **1983**, *37*, 449. Giese, B. *Angew. Chem., Int. Ed. Engl.* **1977**, *16*, 125.

0001-4842/92/0125-0352$03.00/0